DOI: 10.1021/ma102095b

Macromolecules
ARTICLE

Microscopic Observation of Aging of Silica Particles in Unvulcanized Rubber

Yuya Shinohara,*,†,∥ Hiroyuki Kishimoto,†,‡ Naoto Yagi,§,∥ and Yoshiyuki Amemiya†,⊥,∥

†*Department of Advanced Materials Science, The University of Tokyo, 5-1-5 Kashiwanoha, Kashiwa, Chiba 277-8561, Japan,* ‡*Sumitomo Rubber Industries Co., Ltd., Kobe, Japan,* §*JASRI/SPring-8, Hyogo, Japan, and* ⊥*Department of Advanced Materials Science, The University of Tokyo, 5-1-5 Kashiwanoha, Kashiwa, Chiba 277-8561, Japan.* ∥ *CREST/JST*

Received September 10, 2010; Revised Manuscript Received October 7, 2010

ABSTRACT: The dynamics of silica particles in unvulcanized rubber is investigated by X-ray photon correlation spectroscopy (XPCS). The results show the aging behavior of the dynamics; the dynamics of particles slows down as the aging time increases. This slowing down is not accompanied by a change in the configuration of aggregates in size scales of micrometers and sub-micrometers. The aging behavior depends on the type of silane coupling agent and the volume fraction of silica particles, while it does not originate from vulcanization. This study shows that complex microrheological phenomena occur even in industrial products. The relationship between these microrheological phenomena and macroscopic viscoelasticity is an open question.

Introduction

Many soft materials, including colloidal gels, concentrated emulsions, and foams, show slow relaxation processes that resemble the glassy dynamics observed in disordered materials, such as spin glasses and polymer melts.[1,2] Most of these materials are out of thermodynamical equilibrium: for systems far from equilibrium, evolution of the mechanical and dynamical properties with time is observed, in analogy with the slowing down of the dynamics in hard glasses. This slowing down of the properties with time is commonly called aging.[3,4] To elucidate the mechanism of aging in soft materials, many experimental,[5−16] theoretical,[17,18] and numerical studies have been performed. The mode-coupling theory (MCT) has been successfully applied to, for example, colloidal suspensions interacting via a hard-sphere potential,[3] and attempts have been made to extend its validity to concentrated/dilute systems with attractive interactions.[19,20] The concept of dynamical heterogeneity has recently emerged as a key feature of the slow dynamics of glassy systems,[21,22] and many theories have been developed on the basis of or incorporating dynamical heterogeneity.[2,23]

Aging behavior has been experimentally observed in many systems by diffusing wave spectroscopy,[6,9,24] light scattering,[25,26] particle-tracking microrheology,[14,16] and linear rheology experiments.[7,27,28] In all cases, the characteristic time τ continuously increases with sample age t_w. Aging laws, however, highly depend on the type of material investigated. In many cases, the power law $\tau \sim t_w^{\mu}$ is observed, while the aging exponent μ significantly varies. Values of about unity,[5,6,9,27] smaller than unity,[7,28] and larger than unity[11,24] have all been observed. These values reflect full aging, subaging, and hyperaging, respectively. The underlying physics of these phenomena has still not been clarified.

In addition to the academic viewpoint described above, aging phenomena have attracted attention in the field of industrial products. As an example, we take rubber filled with nanoparticles. Tire manufacturers constantly attempt to reduce the rolling resistance of their products to reduce environmental impact by minimizing the use of fossil fuel. However, care must be taken so that the improvement in rolling resistance does not reduce incompatible performance characteristics, such as wet traction. Indeed, tire rolling resistance and wet traction are both determined by energy losses but encompass different deformation magnitudes and frequencies. Rubber filled with nanoparticles is widely used in various products, such as tires of vehicles. To develop rubberlike materials with viscoelastic responses upon deformation such that the above seemingly incompatible properties are fulfilled, nanoparticles, such as carbon black and silica, are generally added to rubberlike materials. This addition of nanoparticles induces considerable improvement in mechanical properties, called the "reinforcement effect", and is essential to the utilization of rubber.[29,30] The mechanism of the reinforcement effect is a controversial issue, although a large number of investigations have been performed by rheological measurements and structural analyses with transmission electron microscopy and X-ray/neutron scattering. In the course of rubber product fabrication, raw rubber is mixed with nanoparticles and ingredients; then, it is heated to a vulcanization temperature and is kept at that temperature until rubber polymers are cross-linked. In the mixing process, the configurations of the nanoparticles are out of equilibrium and are under a complex stress field; this leads to the time evolution of the mechanical properties of the compounds. Indeed, it is known that the Mooney viscosity of unvulcanized rubber increases upon storage.[31] This increase has long been considered as being caused by the cross-linking of the polymers with sulfur atoms. In a recent study, the coalescence of blobs of bound rubber or the reagglomeration of filler particles was proposed to be the origin of this increase in Mooney viscosity.[31,32] On the basis of the above assumption, Lin et al. reported that the Mooney viscosity of the compounds changes upon storage with aging and that the evolution of Mooney viscosity highly depends on the type of added agent.[33] These studies used macroscopic rheological measurement to investigate the aging behavior; however, the direct observation of microscopic spatial and temporal structures was not performed. The use of X-rays to measure both the aggregated structure of nanoparticles and their dynamics will

*To whom correspondence should be addressed. E-mail: yuya@k.u-tokyo.ac.jp.

 Published on Web 10/26/2010

Table 1. Sample Codes (Vulcanized Samples Denoted by v)

	S69-5(v)	S69-20(v)	S363-5(v)
SBR	100	100	100
silica	11.5	54.5	11.5
Si69	0.92	4.36	
Si363			0.92
stearic acid	2	2	2
sulfur	1.5	1.5	1.5
acc TBBS	1	1	1
acc D	1	1	1

provide significant information about the microscopic nature of aging in filled rubber.

Understanding of the microscopic dynamics will help elucidate the mechanism of the complex viscoelastic behavior of filled rubber. Recently developed microrheology techniques are major tools for elucidating the dynamics of particles in complex fluids. Dynamic light scattering (DLS)[34] has been widely used to observe the dynamics of colloidal systems as well as their aging behaviors. The DLS technique for colloidal particles is well established; however, it is not suitable for the observation of the dynamics of nanoparticles in rubber because rubber is almost completely opaque in the wavelength range where conventional DLS is performed. The use of X-rays as a probe is promising for investigating the dynamics of filled rubber. DLS using X-rays, called X-ray photon correlation spectroscopy (XPCS),[35] has attracted much attention and has been utilized as a method to investigate the slow dynamics of soft materials.[36,37]

On the basis of the above background, our goal is to understand the microscopic mechanism of the reinforcement effect: what is the relationship between the microscopic dynamics of particles and macroscopic viscoelastic properties? To reach this goal, in this study, we aim to observe the microscopic dynamics of particles in unvulcanized rubber by XPCS. As a first step, we investigate the aging behavior of styrene−butadiene rubber filled with commercial-grade silica particles. Then, we focus on the change in dynamics during aging by XPCS observation. We choose two types of silane coupling agent: sulfur-functional organosilane Si69 and Si363. Si69 has been widely used as one of the key products in next-generation tires with significantly improved wet grip and rolling resistance, while Si363 is recognized as a successor of Si69 as a silane coupling agent.[38,39] The results clearly indicate the dependence of aging behavior on the type of silane coupling agent and the volume fraction of particles in rubber.

Materials and Methods

Materials. Styrene−butadiene rubber (SBR) samples filled with silica particles were used. The detailed contents of the samples are presented in Table 1. A commercial-grade silica, called Ultrasil VN3, was used as silica particles. The average size of primary particle was determined to be ∼13 nm from TEM observation. We prepared three types of samples for XPCS measurements. The first one was SBR filled with silica particles of 5% v/v, and bis(3-triethoxysilyl)propyl) tetrasulfide ($(C_2H_5O)_3Si(CH_2)_3S_4(CH_2)_3Si(OC_2H_5)_3$: denoted by Si69) was used as a silane coupling agent. The second one was SBR filled with silica particles of 20% v/v, and Si69 was used as a silane coupling agent. The third one was SBR filled with silica particles of 5% v/v, and 3-mercaptopropyltriethoxysilane reacted with ethoxylated C_{13}-alcohol ($(C_2H_5O)[C_{13}H_{27}O(C_2H_4O)_5]_2SiCH_2CH_2CH_2SH$: denoted by Si363) was used as a silane coupling agent. For all the samples, the mixing procedure was the same; the particles and the ingredients were added to raw rubber, and then the compounds were mixed together in an internal mixer until the temperature of the compounds reached 150 °C. Immediately after the mixing process, all the samples were immersed in liquid nitrogen inside a dewar flask; then the samples were brought to a beamline at which XPCS measurements were performed. At the beamline, we took the samples out of the dewar flask and stored them at ambient temperature. The time elapsed since the samples were taken out of the dewar flask was defined as the aging time t_w. This time interval can be considered to be the time interval between the mixing and XPCS measurements under the assumption that the structure and dynamics of silica particles in rubber were unchanged when stored in the dewar flask filled with liquid nitrogen.

It was difficult to cut the samples to make their thickness homogeneous because they were not vulcanized. This prevented us from conducting the detailed structural analysis of the samples because the inhomogeneous thickness would have led to erroneous results in the data reduction procedure of scattering analysis. Thus, we prepared vulcanized samples for structural analysis using X-ray scattering in addition to the XPCS samples; the compounds for X-ray scattering measurement were vulcanized at 150 °C for 35 min to form a sheet of ∼1 mm thickness. The codes of vulcanized samples corresponding to S69-5, S363-5, and S69-20 are S69-5v, S363-5v, and S69-20v, respectively. For each sample, a sheet of raw rubber and a sheet of rubber fully swollen by toluene solution were prepared. The swollen samples were immersed in toluene for over 12 h. The significance of the use of swollen samples is presented in later sections where the results of X-ray scattering are described.

XPCS Measurement. XPCS measurement was carried out at BL40XU,[40] SPring-8 (Hyogo, Japan). The detailed description of the XPCS setting at this beamline is presented elsewhere.[41] Quasi-monochromatic X-rays from a helical undulator were used to perform XPCS. This technique enabled us to use a high-flux-density X-ray beam of 10^{17} photons/(s mm^2). A pinhole of 3 μm diameter was installed 150 mm upstream of the sample to select a partially coherent X-ray beam. The parasitic scattering was removed at a second pinhole that was installed immediately upstream of the sample. By using an interline charge-coupled device (CCD) detector (C4880-80, Hamamatsu Photonics Co., Ltd.) coupled with an image intensifier,[42] two-dimensional X-ray scattering speckle patterns were recorded. The distance between the sample and the detector was ∼3 m. The X-ray energy was 10.5 keV. In this setting, scattering in a q-range of 1×10^{-2}−6×10^{-2} nm^{-1} was recorded, where $q = 4\pi/\lambda \sin\theta$ is the magnitude of the scattering vector and λ and 2θ are the wavelength of X-rays and the scattering angle, respectively. The small longitudinal coherence length due to the quasi-monochromaticity of X-rays limited the observation of speckles to a q-range of 1×10^{-2}−5×10^{-2} nm^{-1}; thus, we analyzed the speckle patterns in this q-range. We successively recorded the speckle images with an exposure time of 436 ms.

For all samples, we define the sample age t_w as the time elapsed since the sample was first placed at ambient temperature at the beamline. To avoid any unintentional effect on the dynamics, we carefully set the sample on a sample stage. We found that even gently touching on the samples resulted in the disturbance of sample dynamics; this led to the lack of the reproducibility of XPCS measurement. All the measurements were performed at room temperature.

In the data reduction process, we first subtracted an average dark image from the data image. The average dark image was calculated using 1000 dark images. Then, we normalized all the data images using the total scattering intensity over each image. This process compensated the intensity fluctuation of the incident X-ray. Subsequently, the ensemble-averaged intensity autocorrelation function $g^{(2)}(q,t)$ was calculated as

$$g^{(2)}(q,t) = \frac{\langle I(q,t_0)I(q,t_0+t)\rangle}{\langle I(q)\rangle^2} \quad (1)$$

USAXS and SAXS Measurements. Nanoparticles in rubber generally show a hierarchical structure; thus, the measurement of scattering over a wide q-range is required to obtain the structural information on nanoparticles in rubber. We performed the

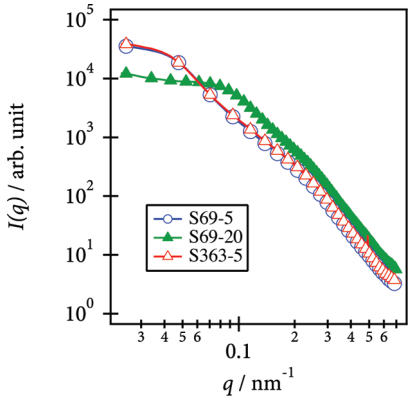

Figure 1. SAXS intensity profiles of S69-5 (open circles), S69-20 (closed triangles), and S363-5 (open triangles).

scattering experiment at different beamlines to cover a wide q-range. Two-dimensional ultrasmall-angle X-ray scattering (2D USAXS) measurement was performed at BL20XU, SPring-8 (Hyogo, Japan). The detailed setting and characteristics of USAXS at this beamline were presented elsewhere.[43] Samples were placed in a hutch in the ring building, and a detector was placed in a hutch in the Biomedical Imaging Center. A cooled CCD detector (C4880-40-26A, Hamamatsu Photonics Ltd.) coupled with an X-ray image intensifier (V7339P, Hamamatsu Photonics Ltd., XRII)[44] was used to record the 2D-USAXS images. The distance between the sample and the detector was 160.5 m, and the X-ray energy was 23 keV. In this setting, the scattering in a q-range of 1.5×10^{-3}–2.5×10^{-2} nm^{-1} was measured. To enlarge the dynamic range of the scattering intensity, we placed a circular attenuator of aluminum immediately upstream of the detector to attenuate the high scattering intensity at the center of the image. The intensity of scattering profiles in the attenuated region was corrected in the data reduction process.

A structure in a smaller size scale was investigated by small-angle X-ray scattering (SAXS) measurement at BL03XU and BL40B2, SPring-8. The pixel detector PILATUS[45] was used to record SAXS images. The distance between the sample and the detector was ~3 m at both beamlines. This distance was calibrated using the positions of the diffraction peaks of standard samples, namely, silver behenate and rat tail collagen. The X-ray energy used was 8 keV. In this setting, the scattering in a q-range of 1.5×10^{-2}–1 nm^{-1} was measured. SAXS intensity profiles of both vulcanized and unvulcanized samples prepared for XPCS were measured.

All the 2D USAXS and SAXS images showed isotropic patterns and thus were azimuthally averaged to obtain one-dimensional scattering intensity profiles. After conventional data reduction processes, the USAXS and SAXS intensity profiles were combined to show scattering intensity profiles over a wide q-range.

Results

USAXS−SAXS Results. From USAXS−SAXS measurements, we obtained structural information on silica particles, such as the structural differences between the samples, the structural change associated with aging, and the dispersive unit of silica aggregates in rubber. Figure 1 shows the SAXS intensity profiles of S69-5, S69-20, and S363-5 obtained at BL03XU. All the intensity profiles show shoulder patterns at ~0.25 nm^{-1}. For S69-20, another shoulder was found at approximately q = 0.09 nm^{-1}, while it was observed at ~0.03 nm^{-1} for S69-5 and S363-5. As described in the previous section, the inhomogeneity in the thickness of unvulcanized samples made it difficult to complete the detailed structural analysis. Thus, we first analyzed the USAXS−SAXS of vulcanized samples to clarify the structure of the unvulcanized samples. The USAXS−SAXS intensity profiles of the vulcanized

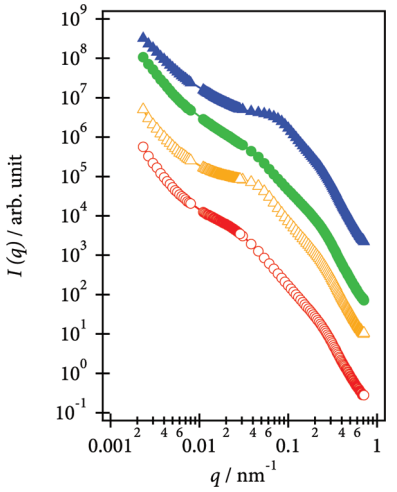

Figure 2. USAXS−SAXS intensity profiles of vulcanized rubber and swollen rubber: S69-5v (circles) and S69-20v (triangles). The open symbols show the results of swollen samples while the closed symbols show those of raw samples. The increase in scattering intensity toward a lower angle (q < 0.01 nm^{-1}) indicates the existence of a larger scale structure. The shoulders observed at ~0.05 nm^{-1} for the swollen S69-20v and that at 0.08 nm^{-1} for the raw S69-20v correspond to the interference between the neighboring aggregates. The small shoulders observed at ~0.03 nm^{-1} for S69-5v correspond to the size of the aggregates. The shoulders at ~0.25 nm^{-1} originate from the form factor of the primary particles.

samples are shown in Figure 2. In this figure, the USAXS−SAXS intensity profiles of S69-5v and S69-20v are shown. All the scattering intensity profiles indicate the presence of a hierarchical structure over a wide q-range. To interpret the characteristics of such a hierarchical structure, a unified fitting approach developed by Beaucage and co-workers has been widely applied.[46−48] Although the analyses using the unified equation is highly effective to interpret the scattering intensity profiles of hierarchical structure, the analyses of interacting aggregates should be performed with great care because there is no interaction term relating to the correlation between aggregates in the unified equation. To overcome this difficulty, Oberdisse et al.[49] have recently reported an appropriate method for analyze interacting aggregates by combining conventional SAXS analysis and reverse Monte Carlo modeling.[50] When the silica particles are spheres with a monodisperse size distribution and form monodisperse aggregates, the scattering intensity $I(q)$ is expressed as the product of contrast $\Delta\rho$, the volume fraction of spheres ϕ, the volume of single sphere V, and the structure and form factors of individual spheres $P(q)$:

$$I(q) = \Delta\rho^2\phi V S_{\mathrm{inter}}(q) S_{\mathrm{intra}}(q) P(q) \qquad (2)$$

where the structure factor is separated to the intra-aggregate structure factor $S_{\mathrm{intra}}(q)$ and the structure factor describing the center-of-mass correlations of aggregates $S_{\mathrm{inter}}(q)$.[49] When the particles and aggregates are not monodisperse spheres as in the present study, the factorization of $I(q)$ into the form and structure factor is impossible. Nevertheless, we can extract the structural information on our sample that is required for the interpretation of XPCS results using the above formalism as follows. Note that detailed structural analysis using elaborate methods is not our interest in the present study; such an analysis will be reported in the near future.

We now analyze the characteristics of the scattering intensity profiles shown in Figure 2 in detail. First, we focus on the scattering profiles in a larger angle region ($q > 6 \times 10^{-3}$ nm^{-1}). For S69-5v, a small shoulder appears at ~0.25 nm^{-1}, while

another shoulder is noticeable at ~0.03 nm^{-1}. The position of the outer shoulder fairly agrees with the Guinier region calculated from the size of primary particles taking the polydispersity of particles. From these results, first, we can conclude that silica particles have two structural levels in this q-range: the primary particles and the aggregates being composed of the primary particles and that the shoulders at approximately 0.25 and 0.03 nm^{-1} reflect the sizes of primary particles and aggregates, respectively. The swelling of the samples with toluene results in a negligible change in their USAXS−SAXS intensity profiles. The changes of the profiles owing to the swelling must be associated with $S_{inter}(q)$, not with the product of $S_{intra}(q)$ and $P(q)$. The fact that the profiles of S69-5v do not show significant changes in this q-range means that $S_{inter}(q)$ does not change its form, indicating that silica aggregates do not interact in a small length scale. There is no peak due to the correlation between the aggregates; this observation also supports the above suggestion. Thus, we can conclude that the aggregates are sparsely dispersed in the SBR matrix and are the dispersive unit of VN3. In a smaller angle region ($q < 6 \times 10^{-3}$ nm^{-1}), an upturn toward a smaller angle is observed in the intensity profiles. The existence of the upturn shows the presence of a larger scale structure. We cannot determine the configurations of this larger scale structure in detail owing to the limited q-range of scattering measurement. There were stains on the surfaces of the samples which might have been the source of the larger scale structure.

Different characteristics were observed for the USAXS−SAXS intensity profiles of S69-20v, as shown in Figure 2. Both raw and swollen samples show a shoulder at ~0.25 nm^{-1} in their scattering intensity profiles; the position of this shoulder agrees with that observed for S69-5v, and thus these shoulders reflect the sizes of their primary particles. Another shoulder, or rather a peak, is apparent at a lower angle. For the raw sample, the shoulder is located at $\sim 8 \times 10^{-2}$ nm^{-1}, while that of the swollen sample is located at $\sim 5 \times 10^{-2}$ nm^{-1}. These shoulders correspond to the interference between the neighboring aggregates described by $S_{inter}(q)$. It is natural to consider that the profile of $S_{intra}(q)P(q)$, which corresponds to the shape and size of the dispersive unit (aggregate), is independent of the volume fraction of silica particles and that the swelling of the samples with toluene should increase the distances between the neighboring aggregates, leading to the change in $S_{inter}(q)$. Thus, the aggregates directly interact with each other in S69-20v, and the scattering in this q-range reflects both the interaction between aggregates and the form of aggregates. For S69-20v, an upturn at a smaller angle ($q < 6 \times 10^{-3}$ nm^{-1}) is also observed in the intensity profiles. The volume fraction of silica particles for S69-20v is high; thus, it is natural to conclude that some larger structures, such as agglomerates, are present. It is, however, difficult to elucidate the configuration of this larger scale structure; thus, we do not discuss its details.

On the basis of the above results, we interpret the result shown in Figure 1. There is no noticeable difference observed between the scattering intensity profiles of S69-5 and S363-5. Thus, the difference in the type of silane coupling agent used does not affect the structure in this size scale. The scattering intensity profiles of S69-5 and S69-20 are similar to those of vulcanized samples. By analogy with the results of vulcanized samples, we can conclude that (1) the shoulder at ~0.25 nm^{-1} corresponds to the size of primary particles as in the vulcanized samples, (2) the shoulder at ~0.03 nm^{-1} for S69-5 and S363-5 reflects the size of aggregates, and (3) the shoulder at ~0.09 nm^{-1} is attributed to the interference between the aggregates. The q-range observed in the XPCS

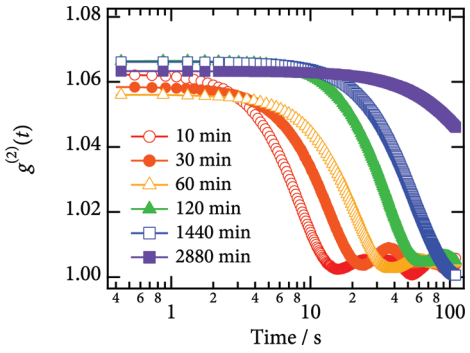

Figure 3. Profiles of normalized intensity-correlation functions of S69-5 at $q = 2.3 \times 10^{-2}$ nm^{-1}. As the aging time increases, the relaxation becomes slower.

described in the following section is 1×10^{-2}−6×10^{-2} nm^{-1}, and the observed scattering is mainly due to the dispersive unit (S69-5 and S363-5) and the combination of the dispersive units and their interferences (S69-20) from the USAXS−SAXS results.

XPCS Results. Figure 3 shows typical intensity-correlation curves of S69-5. As the aging time t_w increases, the relaxation time increases and the dynamics becomes slow. With regard to the oscillations of signal at around 20−40 s, experimental noises would be the origin, which should be investigated in the future work. We fit the initial relaxations of these intensity-correlation curves using compressed exponential functions:

$$g^{(2)}(q,t) = 1 + A \exp\left(-2\left(\frac{t}{\tau}\right)^{\beta}\right) \quad (3)$$

The q-dependence of the relaxation time τ of S69-5 is shown in Figure 4A. As the aging time increases, the relaxation time increases. No clear change in the power law with the evolution of t_w is observed, which is discussed in the next section in detail. The best-fit values of exponent β are shown in Figure 4B. No dependence of β on q is observed, although the values are sparsely dispersed around the average value except for those of $t_w = 2160$ min. When $t_w = 2160$ min, the value of β increases with q. When the aging time is small, around $t_w < 360$ min, the values of β are around 2.0−2.2, indicating the ballistic or superdiffusive motion of particles. At a longer aging time, the values of β decrease.

For S69-20 and S363-5, the fitting of the initial relaxation of intensity-correlation curves using compressed exponential functions was performed. The results of fitting for S69-20 and S363-5 are shown in Figures 5 and 6, respectively. The q-dependence of the relaxation time τ of S69−20 shows different behavior from that of S69−5. The q-dependence of S69-5 shows a clear power law, while that of S69-20 shows complex behavior. The values of β are generally smaller than those for S69-5. There is a tendency that the values of β decrease as the aging time increases, although they are sparsely dispersed. Figure 6 shows that the q-dependence of τ of S363-5 is similar to that of S69-5, while the relaxation time of S363-5 is larger. The q- and t_w-dependences of β generally show a tendency similar to that of S69-5.

To eliminate the possibility that the t_w-dependence of the dynamics originates from the change in the structure in the same size scale, such as that due to the aggregation of particles, we analyzed the scattering intensity profiles of XPCS data during the aging process by azimuthally averaging the two-dimensional scattering speckle images so that

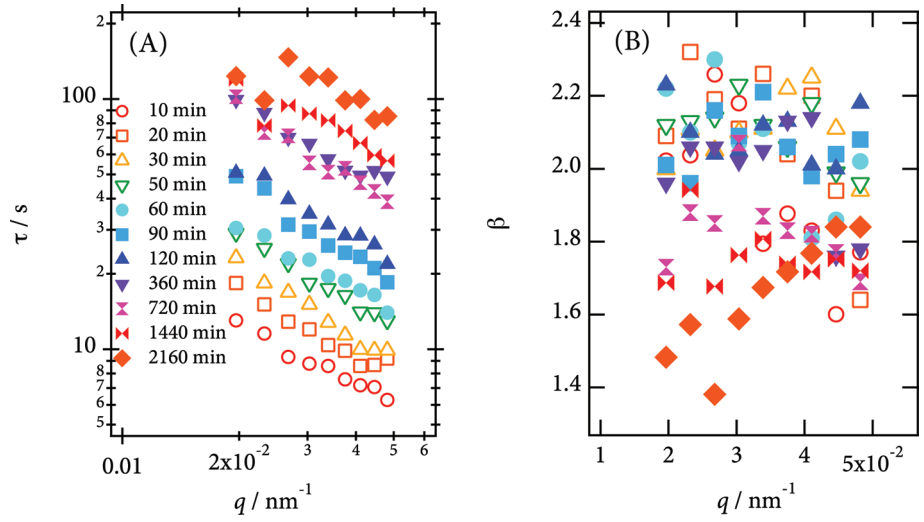

Figure 4. (A) Relaxation time τ vs scattering vector q for S69-5. The different symbols indicate different aging times. (B) Exponent β vs scattering vector q.

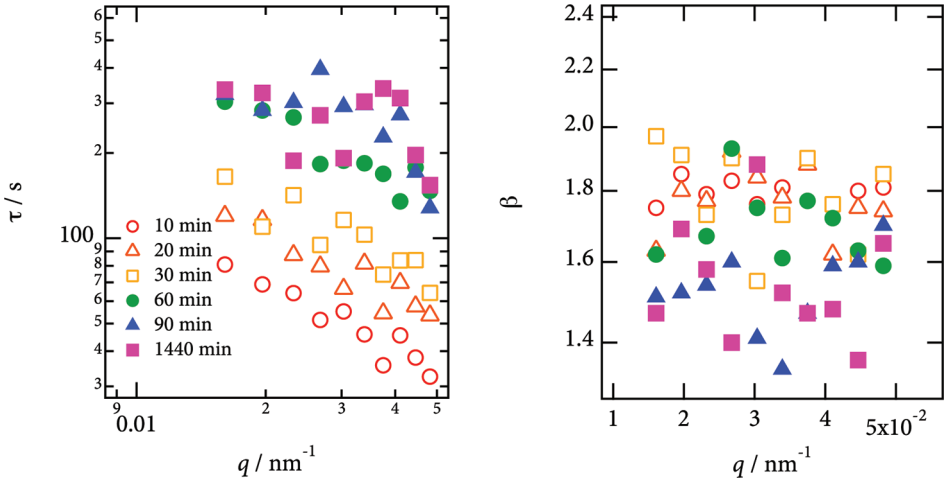

Figure 5. (A) Relaxation time τ vs scattering vector q for S69-20. The different symbols indicate different aging times. (B) Exponent β vs scattering vector q.

scattering profiles without speckles are observed. The averaging process was performed on 999 successive images. Figure 7A−C shows the average scattering intensity profiles of S69-5, S69-20, and S363-5, respectively. These results indicate that there is a negligible difference among the profiles at different aging times. From these results, we can conclude that the aggregation does not proceed during this aging process, and thus the change in the dynamics does not originate from any aggregation in this size scale. Note that the present result does not eliminate the possibility that a change in the larger scale structure induces the change in the dynamics.

Discussion

From the above results, the dynamics of particles slows down as the aging time increases. As shown in Figures 4A, 5A, and 6A, the q-dependence of the relaxation time shows single-power-law behavior, although the fitting starts to fail at a large t_w with regard to S69-20. To analyze the change in slope, the best-fit value of α defined by the following equation is shown in Figure 8:

$$\tau = Cq^{-\alpha} \tag{4}$$

The values of α for S69-5 are almost constant at ~1.0. For S363-5, the results show a similar tendency, although they are sparsely dispersed compared with those of S69-5. These results indicating $\alpha \sim 1$ show that the dynamics of the particles is described by ballistic motion. For S69-20, the value of α decreases as the aging time increases and becomes around 0.3 at $t_w = 1440$ min. This behavior is particularly unusual when we observe that $\alpha = 2$ for simple diffusive behavior; the dynamics is particularly "superdiffusive". We cannot give clear descriptions of the nature and mechanism of this peculiar dynamics. A large volume fraction and the overlapped measurement of self-diffusion and collective diffusion would affect this behavior because the observed scattering for S69-20 is due to the combination of the dispersive units and their interference as described in the previous section. At t_w = 1440 min, the profile shows a peak at around $q = 4 \times 10^{-2}$ nm^{-1} in Figure 5A. This slowing down might be attributed to the so-called "de Gennes narrowing": a slowing down in the decay of the autocorrelation function at the peak position of structure factor, which in turn has its origins in the strong spatial correlations existing at the peak position.[51] The first peak of the structure factor, however, is located at a larger q, around 9×10^{-2} nm^{-1}, which is outside the available q-range; thus, further studies on a larger q are required to clarify the existence of this effect so as to check whether the observed dynamics is collective.

To analyze the slowing down of particle dynamics quantitatively, we define the quantity corresponding to the particle

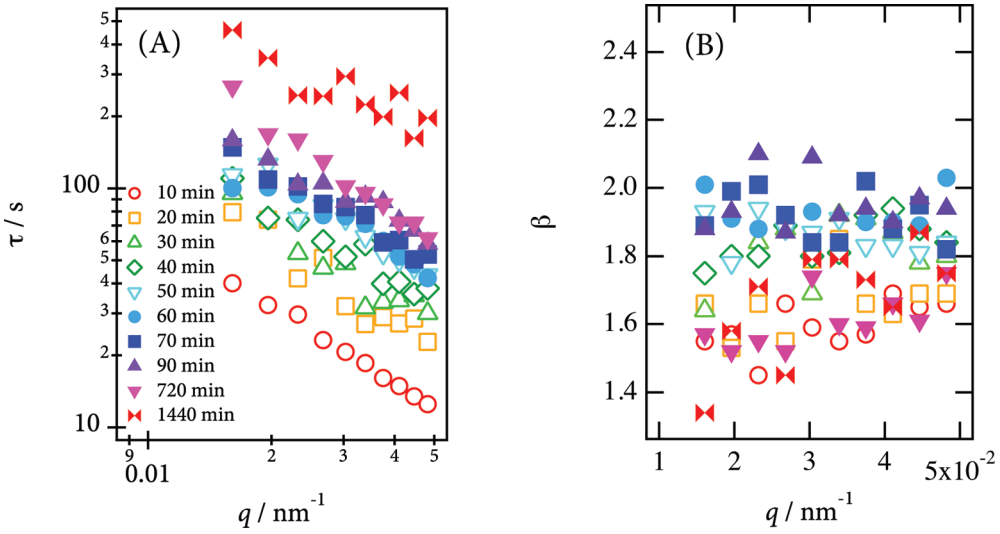

Figure 6. (A) Relaxation time τ vs scattering vector q for S363-5. The different symbols indicate different aging times. (B) Exponent β vs scattering vector q.

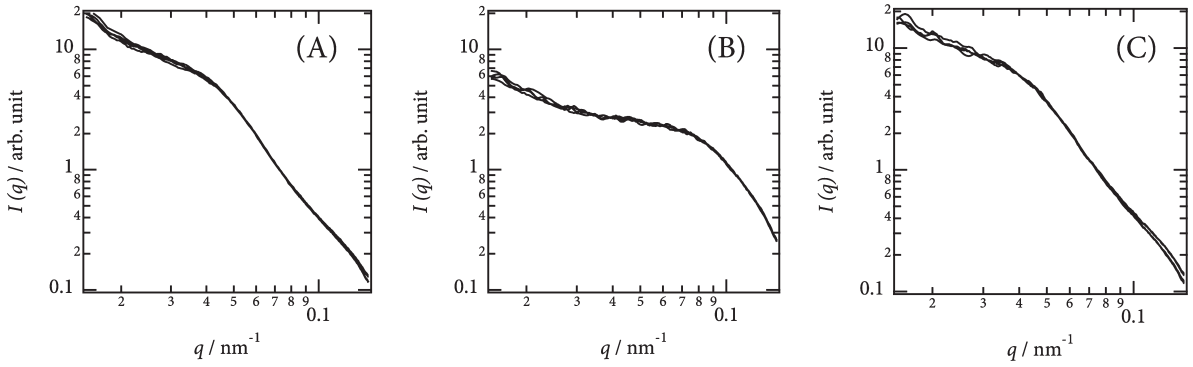

Figure 7. SAXS intensity profiles during aging process: (A) S69-5, (B) S69-20, and (C) S363-5. The aging times were 10, 30, 60, 90, and 120 min. There is a negligible difference among the intensity profiles at different aging times t_w; thus, we do not distinguish the profiles in these figures. The absence of a difference indicates that there is no apparent change in the average structure of aggregates while the relaxation time changes.

velocity for S69-5 and S363-5 at each t_w by calculating the inverse of the product of q and τ:

$$v = (q\tau)^{-1} \tag{5}$$

The results are shown in Figure 9; a clear slowing down is observed for both S69-5 and S363-5. The values of v for S363-5 are smaller than those for S69-5. The difference in v between S69-5 and S363-5 is solely due to the type of silane coupling agent; thus, it can be concluded that the difference in interaction between silica and rubber polymers through a silane coupling agent greatly affects the dynamics of silica aggregates. With regard to S69-20, the deviation of α from unity is large, and we cannot compare the aging behavior with other samples by calculating the velocity of particles (eq 5) at present; further theoretical considerations are required to quantitative discussion of the aging behavior of S69-20.

The dynamics of S69-5 and S363-5 monotonically slowed down. The slowing down behavior of S69-5 is well fitted with a power law, as indicated by the line in Figure 9:

$$v \sim t_w{}^{-0.5} \tag{6}$$

Regarding the origin of this aging behavior, we do not have a clear picture at present. In the following, we try to give a qualitative explanation, which is based on the results of the

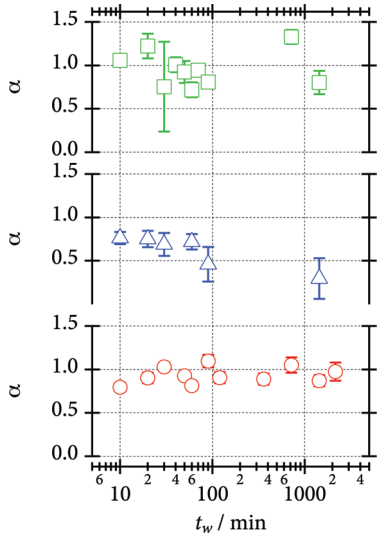

Figure 8. Dependence of α on aging time t_w: S69-5 (circles), S69-20 (triangles), and S363-5 (squares).

previous studies.[5,18] As described in the Materials section, silica particles were mixed in a mixer. The relaxation time of polymer chains should be much shorter than the time interval between the mixing process and the earliest XPCS measurement, particularly

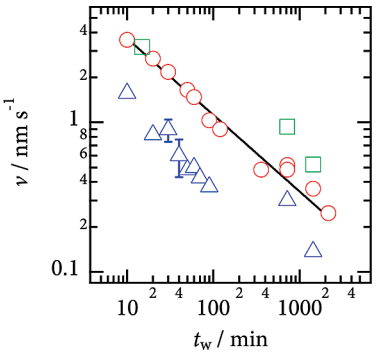

Figure 9. Dependence of v on aging time t_w: S69-5 (circles), S363-5 (triangles), and S69-5 without sulfur (squares). The lines indicates the best-fit result of S69-5 obtained using a power function ($v \sim t_w^{-0.5}$).

under the condition that the polymer chains are not vulcanized; thus, the relaxation of polymer chains does not affect the present aging behavior, or at least, its effect is expected to be very small. What affects the aging behavior must be the configuration of aggregates (dispersive units) and their hydrodynamic interaction. Immediately after the mixing process, the configuration of aggregates must be far out of equilibrium, and each aggregate is under a complex strain field; this strain field originates from the displacement of surrounding particles. The restructuring of the elastic network should occur owing to the random, local shrinking of the network and the associated development of heterogeneous residual stresses in it that relax with time. When one particle moves due to the strain field, its displacement is transmitted to surrounding particles through polymer chains as a strain field, resulting in the displacement of surrounding particles. As this process repeats continuously, the local configuration of the aggregates changes so as to release the strain on the individual aggregates and to reach the equilibrium state; then, the strain field inducing the displacement of the aggregates is reduced, and the velocity of each aggregate decreases. We have to keep in mind that the scattering intensity profiles do not change during the aging process, as shown in Figure 7. This observation that the scattering intensity profiles do not change does not conflict with the above discussion. What is observed in the present scattering experiment corresponds to the average structure of neighboring aggregates. The average structure as a whole does not change even if the configuration of the individual aggregates changes.

Sulfur was included in the samples; thus, it is possible that cross-linking by sulfur (vulcanization) occurs and that it induces the slowing down of the dynamics. To eliminate this possibility, we performed the same type of XPCS measurement for S69-5 that does not contain sulfur. The $g^{(2)}(t)$ for this sample shows behavior similar to that of the sample containing sulfur, and the dependence of v on t_w is shown in Figure 9. The values of v agree well with those of S69-5 containing sulfur. Thus, the dynamics observed in the present study is not due to cross-linking during aging but originates from the mechanism described above.

The detailed analysis of dynamics with regard to S69-20 requires the separation of collective motion and self-motion. This also requires the use of model samples, such as monodispersive spherical particles embedded in rubber. Thus, the XPCS study of particles with a high volume fraction should be performed using a model sample containing monodisperse spheres. For further analysis, the relationship between the dynamics of particles and the polymer structure is a matter of interest. In the present system, not only do the aggregates hydrodynamically interact with each other but also polymer chains entangle and interact with particles. Because the silane coupling agent generally connects the interface of silica with polymer chains, the structure and dynamics of rubber itself are important. The relationship between the polymer structure and the dynamics of particles is an open question.

To elucidate the detailed aging behavior, XPCS measurements over a much wider q-range are required, which will be performed in the near future. To measure the dynamics in a smaller q-range, a recently proposed method using near-field speckles[52] is a major candidate. Radiation damage is always a serious problem in the XPCS measurement of soft materials. The use of speckle visibility spectroscopy[53] with X-rays will offer the same information as XPCS with lower radiation damage. Further investigation regarding the macroscopic aging behavior will be performed with these novel methods and will clarify the relationship between the microscopic dynamics and macroscopic viscoelasticity; this understanding will enable us to understand the mechanism of the reinforcement effect.

Conclusion

We observed the aging behavior of silica particles in rubber by X-ray photon correlation spectroscopy. The results show that the dynamics of particles slows down as the aging proceeds, while the structure of the particles does not change during the process. The slowing down does not originate from vulcanization. The difference in the type of silane coupling agent used induces the difference in interaction between silica particles and rubber polymers; this results in the different behavior of the dynamics. The increase in the volume fraction of silica particles brings about peculiar dynamics, which requires further investigation.

Acknowledgment. The authors thank Drs. N. Ohta, H. Masunaga, Y. Suzuki, A. Takeuchi, and K. Uesugi (JASRI/SPring-8) for their kind help in performing USAXS, SAXS, and XPCS experiments. The XPCS experiments were performed under the approval of the SPring-8 Proposal Advisory Committee (Proposals 2007A1797, 2007B1060, 2009B1055, and 2010A1109). The USAXS and SAXS experiments were also performed under the approval of the SPring-8 Proposal Advisory Committee (2007B003, 2007B004, 2008A003, 2008A004, 2009B1095, and 2010A7217).

References and Notes

(1) *Soft and Fragile Matter*; Cates, M., Evans, M., Eds.; Institute of Physics Publishing: London, 2000.
(2) Cipelletti, L.; Ramos, L. *J. Phys.: Condens. Matter* **2005**, *17*, R253–R285.
(3) Gotze, W.; Sjogren, L. *Rep. Prog. Phys.* **1992**, *55*, 241–376.
(4) Bouchaud, J.-P.; Cugliandolo, L.; Kurchan, J.; Mézard, M. *Physica A* **1996**, *226*, 243–273.
(5) Cipelletti, L.; Manley, S.; Ball, R. C.; Weitz, D. A. *Phys. Rev. Lett.* **2000**, *84*, 2275–2278.
(6) Knaebel, A.; Bellour, M.; Munch, J. P.; Viasnoff, V.; Lequeux, F.; Harden, J. L. *Europhys. Lett.* **2000**, *52*, 73–79.
(7) Ramos, L.; Cipelletti, L. *Phys. Rev. Lett.* **2001**, *87*, 245503.
(8) Bonn, D.; Tanase, S.; Abou, B.; Tanaka, H.; Meunier, J. *Phys. Rev. Lett.* **2002**, *89*, 015701.
(9) Viasnoff, V.; Lequeux, F. *Phys. Rev. Lett.* **2002**, *89*, 065701.
(10) Cipelletti, L.; Ramos, L.; Manley, S.; Pitard, E.; Weitz, D. A.; Pashkovski, E. E.; Johanson, M. *Faraday Discuss.* **2003**, *123*, 237–251.
(11) Bandyopadhyay, R.; Liang, D.; Yardimci, H.; Sessoms, D. A.; Borthwick, M. A.; Mochrie, S. G. J.; Harden, J. L.; Leheny, R. L. *Phys. Rev. Lett.* **2004**, *93*, 228302.
(12) Ramos, L.; Cipelletti, L. *Phys. Rev. Lett.* **2005**, *94*, 158301.
(13) Schosseler, F.; Kaloun, S.; Skouri, M.; Munch, J. P. *Phys. Rev. E* **2006**, *73*, 021401.
(14) Wang, P.; Song, C.; Makse, H. A. *Nature Phys.* **2006**, *2*, 526–531.
(15) Schupper, N.; Rabin, Y.; Rosenbluh, M. *Macromolecules* **2008**, *41*, 3983–3994.
(16) van den Ende, D.; Purnomo, E. H.; Duits, M. H. G.; Richtering, W.; Mugele, F. *Phys. Rev. E* **2010**, *81*, 011404.
(17) Sollich, P.; Lequeux, F.; Hébraud, P.; Cates, M. E. *Phys. Rev. Lett.* **1997**, *78*, 2020.

(18) Bouchaud, J.-P.; Pitard, E. *Eur. Phys. J. E* **2001**, *6*, 231–236.
(19) Dawson, K. A. *Curr. Opin. Colloid Interface Sci.* **2002**, *7*, 218–227.
(20) Kroy, K.; Cates, M. E.; Poon, W. C. K. *Phys. Rev. Lett.* **2004**, *92*, 148302.
(21) Ediger, M. D. *Annu. Rev. Phys. Chem.* **2000**, *51*, 99–128.
(22) Richert, R. *J. Phys.: Condens. Matter* **2002**, *14*, R703–R738.
(23) Duri, A.; Cipelletti, L. *Europhys. Lett.* **2006**, *76*, 972–978.
(24) Bissig, H.; Romer, S.; Cipelletti, L.; Trappe, V.; Schurtenberger, P. *PhysChemComm* **2003**, *6*, 21–23.
(25) Bellour, M.; Knaebel, A.; Harden, J. L.; Lequeux, F.; Munch, J. P. *Phys. Rev. E* **2003**, *67*, 031405.
(26) Abou, B.; Bonn, D.; Meunier, J. *Phys. Rev. E* **2001**, *64*, 021510.
(27) Cloitre, M.; Borrega, R.; Leibler, L. *Phys. Rev. Lett.* **2000**, *85*, 4819–4822.
(28) Derec, C.; Ducouret, G.; Ajdari, A.; Lequeux, F. *Phys. Rev. E* **2003**, *67*, 061403.
(29) Guth, E. *J. Appl. Phys.* **1945**, *16*, 20.
(30) Wang, M. J. *Rubber Chem. Technol.* **1998**, *71*, 520–589.
(31) Schaal, S.; Coran, A. Y. *Rubber Chem. Technol.* **2000**, *73*, 225–239.
(32) Schaal, S.; Coran, A. Y.; Mowdood, S. K. *Rubber Chem. Technol.* **2000**, *73*, 240–252.
(33) Lin, C. J.; Hergenrother, W. L.; Hilton, A. S. *Rubber Chem. Technol.* **2002**, *75*, 215–245.
(34) Berne, B. J.; Pecora, R. *Dynamic Light Scattering*; Dover: Mineola, NY, 2000.
(35) Sutton, M.; Mochrie, S. G.; Greytak, T.; Nagler, S. E.; Berman, K. E.; Held, G. A.; Stephenson, G. B. *Nature* **1991**, *352*, 608–610.
(36) Grübel, G.; Madsen, A.; Robert, A. In *Soft-Matter Characterization*; Borsali, R., Pecora, R., Eds.; Springer-Verlag: Berlin, 2008; Chapter 18, pp 953−995.
(37) Sutton, M. *C. R. Phys.* **2008**, *9*, 657–667.
(38) Klockmann, O.; Hasse, A. *Kauts. Gum. Kunst.* **2007**, *60*, 82–84.
(39) Niedermeier, W.; Schwaiger, B. *Kauts. Gum. Kunst.* **2007**, *60*, 184–187.
(40) Inoue, K.; Oka, T.; Suzuki, T.; Yagi, N.; Takeshita, K.; Goto, S.; Ishikawa, T. *Nucl. Instrum. Methods. Phys. Res., Sect. A* **2001**, *467−468*, 674–677.
(41) Shinohara, Y.; Kishimoto, H.; Maejima, T.; Nishikawa, H.; Yagi, N.; Amemiya, Y. *Jpn. J. Appl. Phys.* **2007**, *46*, L300–L302.
(42) Shinohara, Y.; Imai, R.; Kishimoto, H.; Yagi, N.; Amemiya, Y. *J. Synchrotron Radiat.* **2010**, in press.
(43) Shinohara, Y.; Kishimoto, H.; Inoue, K.; Suzuki, Y.; Takeuchi, A.; Uesugi, K.; Yagi, N.; Muraoka, K.; Mizoguchi, T.; Amemiya, Y. *J. Appl. Crystallogr.* **2007**, *40*, s397–s401.
(44) Amemiya, Y.; Ito, K.; Yagi, N.; Asano, Y.; Wakabayashi, K.; Ueki, T.; Endo, T. *Rev. Sci. Instrum.* **1995**, *66*, 2290–2294.
(45) Broennimann, C.; Eikenberry, E. F.; Henrich, B.; Horiberger, R.; Huelsen, G.; Pohl, E.; Schmitt, B.; Schulze-Briese, C.; Suzuki, M.; Tomizaki, T.; Toyokawa, H.; Wagner, A. *J. Synchrotron Radiat.* **2006**, *13*, 120–130.
(46) Beaucage, G. *J. Appl. Crystallogr.* **1995**, *28*, 717–728.
(47) Beaucage, G.; Ulibarri, T. A.; Black, E. P.; Shaefer, D. W. In *Multiple Size Scale Structures in Silica-Siloxane Composites Studied by Small-Angle Scattering*; Mark, J. E., Lee, C. Y.-C., Bianconi, P. A., Eds.; ACS Symposium Series; American Chemical Society: Washington, DC, 1995; Chapter 9.
(48) Beaucage, G. *J. Appl. Crystallogr.* **1996**, *29*, 134–146.
(49) Oberdisse, J.; Hine, P.; Pyckhout-Hintzen, W. *Soft Matter* **2007**, *3*, 476–485.
(50) McGreevy, R. L. *J. Phys.: Condens. Matter* **2001**, *13*, R877–R913.
(51) de Gennes, P. G. *Physica* **1959**, *25*, 825–839.
(52) Cerbino, R.; Peverini, L.; Potenza, M. A. C.; Robert, A.; Giglio, M. *Nature Phys.* **2008**, *4*, 238–243.
(53) Dixon, P. K.; Durian, D. J. *Phys. Rev. Lett.* **2003**, *90*, 184302.